CERN - EUROPEAN ORGANIZATION FOR NUCLEAR RESEARCH

E

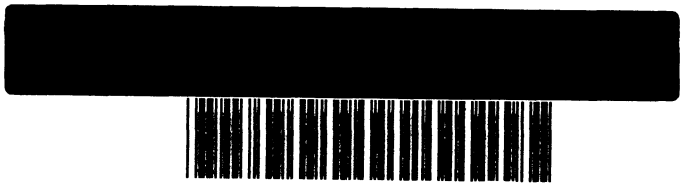

CERN/EF/BEAM 78-2
15 March 1978

WEST AREA NEUTRINO FACILITY-SHIELDING STUDIES

A.L. Grant
CERN, Geneva, Switzerland

1. INTRODUCTION

A new independent calculation of the West Area neutrino beam shielding has been made in order to understand the cause of the direct muon leakage which is resulting in high background levels in BEBC and the experiment WA1. This note describes briefly the technique of the calculation and makes a comparison of the results with the data of the beam tests at 350 GeV/c and 400 GeV/c. The source of the muon leakage is clearly understood in terms of a lack of stopping power of the shield at certain critical angles. It is unnecessary to invoke defects at holes in the mechanical structure of the shield to explain the background effects.

The remaining part of the note discusses the application of the calculation to various options which will allow the primary proton momentum of the wide-band neutrino beam to be raised to 450 GeV/c. In particular a proposal is made for a modification of the present shielding, partly magnetic and partly passive iron, which will give good shielding at 450 GeV/c at a minimum cost.

As the conclusions of the latter part of this note depend largely on the results of the calculation of the effect of the shielding, the methods used and the limitations of any such calculations, will be described in some detail. The form of the calculation is purely analytical, a Monte-Carlo type of sampling could not be expected to give reliable results on effects of the order of one part in 10^{10} at any reasonable level of computer time.

ALG/mk

An essential part of the program is the description of the layout of the muon shield and the surrounding material in the most detailed manner possible. This detail is such as to contain the structure of the detector pits, concrete linings of different densities, and most important, the detailed structure of the foundations and floor in the region where the beam enters the West Area. Additional absorbers, with or without magnetic field, can be inserted at any point. An example of the detail necessary to observe the azimuthal variation of the stopping power of the shield is shown in fig. 1. This figure shows in (a) the momentum left from a 400 GeV/c muon after traversing the shield as a function of the polar angle λ, scanned in a vertical plane at the target (only energy loss due to ionisation is assumed); (b) is a corresponding scan in the horizontal plane. The asymmetries seen in (a) are due to the non-circular shape of the main iron shielding disks and the structure of the floor of the West Area. Left-right asymmetries of the shielding are small, fig. 1(b). The cross-hatched region shows the effect of the 1200 tons of iron added in the Hall E2 in early Summer 1977. Even from this rather simple, purely geometrical study it is clear that the stopping power of the shield is non-uniform with a lack of shielding at an angle of $\sim$ 3 mr to the target.

2. TECHNIQUE OF THE SHIELDING CALCULATION

To study the penetration through the shield, weighted samples of muons are tracked through the detailed structure at fixed intervals of polar and azimuthal angles, account is kept of energy loss, material traversed and multiple scattering. The distribution of muon background at the detector is obtained by integrating over the surviving set of normal distributions from multiple scattering.

The starting weight of the "ray" of muons traced comes from the production of the parent $\pi^{\pm}$ [1](*) modified by the $\pi_{\mu 2}$ decay probability in the potential length available in the decay tunnel. The production spectra for the parent is integrated over the step size in polar angle λ, azimuth angle ϕ and momentum p, typically 0.2 mr π/10 and 10 GeV/c respectively.

(*) The production spectra is taken from the thermodynamic model of Hagadern Ranft. The version used is that modified by the SPS experimental area group.

The "muon ray" is tracked through the horn and reflector into the shield. The focusing power of the horns are parameterised in terms of the point to parallel focused momentum p_F

$$\text{deflection} = \sin \lambda \cdot p_{F/p} \cdot \text{charge}.$$

The value of p_F used is as for the present wide-band beam, 60 and 120 GeV/c respectively.

Once in the shield the "muon ray" is tracked until it reaches the detector or stops from ionisation energy loss. In the tracking procedure steps up to 20 metres can be made, however, the detailed boundaries between materials are found with an accuracy of $\lesssim$ 8 cm. Energy loss of the muons in the iron and earth/molasse shield has been treated in several ways. Total energy loss, including pair production and bremsstrahlung, as defined in ref. [2] was tried but not used as this gives overly optimistic results. Pair production and bremsstrahlung, though giving a large energy loss to some muons, and hence to the mean, are discrete processes with a long radiation length at the energies of interest. Momentum loss due to ionisation is computed from the high energy form given in ref. [2] with a step size dx $\lesssim$ 50 cm.

$$\frac{dp}{dx} = - \frac{A}{\beta} \left[B + 2.34\ 10^{-4}\ \eta - 2.62\ 10^{-8}\ \eta^2 \right]$$

$$A = \rho\ Z/A\ 10^{-3}$$

$$B = 4.55 - 0.1535\ \ell n\ (\rho \times Z/A).$$

This energy loss is used as the criteria of the "muon ray" stopping. However, it gives an unduly pessimistic estimate of the intensity in the ray; many muons are lost from the ray by other processes. To obtain an estimate of the remaining intensity an additional weight is given to the ray. This weight is taken from tabulated curves of integrated stopping

power calculated by a Monte-Carlo program [3](*). An example of these weights compared with total energy loss and ionisation energy loss is shown in table 1.

It must be stressed however that a normalisation derived from this weighting process is very sensitive to the densities, composition, etc. of the shield; for example, a change in the density of the iron shield from 7.2 to 7.3, i.e. 1.4%, changes the weight at 400 GeV/c by a factor of 2.

As an example of the computation of energy loss the momentum spectrum of background muons from the 400 GeV ν beam measured at WA1 is shown in fig. 2. The solid curve, ionisation loss only, is normalised to the experimental data, but fits the shape well. The dashed curve from total energy loss shows the expected underestimate of the hardness of the background spectrum.

The most complex part of the shielding calculation is the correct handling of the multiple Coulomb scattering. The scattering process implies the existence of trajectories which can leave the main shield and following a curving path reach the detector. The conventional treatment of this problem is to calculate a Monte-Carlo "random walk" process. However, due to the complexity and size of the shielding structure in this case, this was not possible apart from a few rays for the purpose of checking the analytical calculation.

As any ray is tracked through the shield, the multiple Coulomb scattering envelope is computed at each step by the form

$$\theta_1^2 = (21/p\beta)^2 \quad dx/X_o$$

$$\langle\theta T\rangle_1 = \theta^2 \, dx/2$$

$$T_1^2 = (dx)^2 \, \theta^2/3,$$

where θ, T and $\langle\theta T\rangle$ are the scattering angle, displacement, and correlation

---

(*) These curves of integrated stopping power of iron and molasse for high energy muons come from a Monte-Carlo program which takes into account the straggling effect due to the discrete energy loss processes written by H. Atherton. The computed results agree well with the measurements made on axis with the present neutrino shield.

due to scattering in step dx in material of radiation length X_o. At each new step i, the scattering is increased with the correlation between θ and T taken into account

$$T^2 = T^2_{i-1} + T^2_i + (dx)^2\ \theta^2_{i-1} + 2.\ dx\ \langle\theta T\rangle_{i-1}$$

$$\langle\theta T\rangle = \langle\theta T\rangle_{i-1} + \langle\theta T\rangle_i + dx\ \theta^2_{i-1}$$

$$\theta^2 = \theta^2_{i-1} + \theta^2_i\ .$$

The starting value of θ is

$$\theta = 0.057/p,\ p \text{ in GeV/c},$$

at the mid-point of the decay potential length to roughly take into account the $\pi_{\mu 2}$ decay angle distribution. The form above assumes only a Gaussian distribution of multiple scattering, the large angle tails of the measured distribution are not considered. This simplification can be justified as the displacement due to scattering is already large with respect to the lateral size of the shielding structure. A typical muon has a σ_{rms} for multiple scattering of $\sim$ 200 cm at BEBC. At the detector the intensity I(y, z) of background muons is obtained by integrating over the many individual two-dimensional scattering distributions

$$I(y,\ z) = \frac{\text{weight}}{2\pi\sigma^2} \int_{YZ} \exp\left(-\frac{y^2+z^2}{2\sigma^2}\right) dydz.$$

Many of the initial studies of the neutrino shielding were made with this tracking of the mean of the multiple scattering distribution; it does not, however, describe the effects shown in figs 3(a) and 3(b). These are (a) the shadowing effect of the main iron for rays which just miss, or (b) the possibility of muons starting well inside the iron,

leaking out sideways and still back-scattering to the detector. These effects are taken into account in the final calculation by tracking each part of the multiple scattering envelope independently. Each weighted "muon ray" is sub-divided into 24 parts, 8 sectors in azimuth and 0-1, 1-2 and > 2 times σ_{rms} for scattering angle. Each sub-division is tracked independently with its particular energy loss about its mean intensity and at each step diverges from the centre of the ray by an amount corresponding to the multiple scattering. At the detector the surviving parts of the now possibly distorted Gaussian distribution are integrated as before (fig. 3(c)).

The success of this procedure may be seen in figs 4 and 5. Fig. 4 shows the predicted intensity distribution on 20 x 20 cm cells of the 350 GeV ν wide-band beam at a plane normal to the direction of the beam at the BEBC-EMI. The plot covers an area of ± 10 m horizontally and ± 5 m vertically. The positions of the External Muon Identifier (EMI) chambers projected on the plane are shown. Fig. 5 shows the projections of this plot at the position of the centre of the upper and lower chambers compared to the measured rate of muons per m^2 per 10^{12} protons. The excess of muons measured at negative y is due to ν induced μ^-, bent by the magnetic field of BEBC. In general the measured asymmetries in the background are fitted by the calculation. The shadowing effect of the main iron absorber in the central region is well described.

3. COMPARISON WITH MEASUREMENTS AT 350 AND 400 GeV

It has been seen from figs 2, 4 and 5 that the computation of the shielding gives a good qualitative description of momentum spectrum and spatial distribution of the background. The same type of intensity plot and projections for the 400 GeV ν beam are shown in figs 6 and 7, in this case with no magnetic field in BEBC. Again the qualitative features of the distribution of background are well described, though it can be seen that the background rate is $\sim$ 10 times higher.

The sum of the weights of the penetrating "muon rays" gives an absolute prediction of the muon background in BEBC and on the EMI. These predictions and the measured rates are summarized in table 2. The rates measured on the EMI have been corrected by subtracting 50 hits for the cosmic ray background per pulse and an estimated number of 8, 1 and 1 ν, $\bar{\nu}$ induced muons per 10^{12} protons for the 350 GeV/c ν, $\bar{\nu}$ and no horn beam. The rate measured for 400 GeV/c neutrino has been similarly corrected. In general the predictions are good to about a factor of two (considering the complexity of the calculation and the many unknowns), this can be considered satisfactory agreement. There is no strong systematic effect in the ratios of measured to predicted rates at 350 GeV indicating that the stopping power of the present shield is well estimated. The ratio of the positive background with 350 GeV $\bar{\nu}$ beam to the mostly negative background with 350 GeV ν is predicted to be 129/23 $\sim$ 6/1, which is what would be expected from the π^+/π^- production spectra. In practice the measured ratio is about 3, indicating that more μ^+ than expected miss the EMI plane. In contrast the prediction for the "no horn" beam is a factor of 2 low, though the background is also mainly positive. The conclusion is that these fluctuations in the predictions by a factor of about two are due mainly to the finite step size in the process of integrating over the multiple Coulomb scattering envelope, and are not in themselves significant.

The background estimate at 400 GeV/c is a factor of three times higher than measured. This could arise due to an overestimate of the production spectra, or more likely, the other processes of energy loss, pair production, bremsstralung, etc. are more effective in stopping muons than the conservative estimate made in [3].

The comparison with the experimental measurements indicate that the calculation describes the properties of the neutrino shield. The spatial and momentum distributions of the background are understood and the absolute rate of background can be predicted to within a factor of $\sim$ 2. It is thus reasonable to have confidence in applying the same technique of calculation to an extension of the shielding for a 450 GeV wide-band neutrino beam.

4. EXTENSION TO 450 GeV

The extension of the present neutrino shielding to handle a 450 GeV wide-band neutrino beam at such a background level to allow useful operation of the BEBC-EMI poses several problems:

(a) The increase of the stopping power of the shield along the beam axis in order to stop the highest energy muons. This implies an additional 18 000 gm/cm^2 of shielding or 36 m of iron replacing earth.

(b) The correction of the present lack of shield at angles $\sim$ 3 mr to the target and the addition of adequate shielding up to angles of $\sim$ 6 mr to the target.

(c) At energies above $\sim$ 400 GeV a new source of muon background appears. Muons, produced even at 0 mr to the target have sufficient energy to multiple scatter out of the main iron shield and still back-scatter to the detector. The shielding requirement tends to overlap with that of (b), but the effect must be considered especially for the magnetic shield discussed later.

Several different shielding layouts satisfying points (a)-(c) have been considered. Arguments on the basis of cost, practicability of civil engineering, and the length of the closure of the neutrino facility, have reduced the available options to two designs which have been studied in depth. These two designs are described in the following sections.

4.1 BRIC-F(*) - Addition of passive iron shielding

The criterion for this design has been to add to the present shield the minimum amount of iron required to give a safe muon shield for 450 GeV primary protons. The constraints on the layout of the shield have come mainly from considerations of simplicity and cost of civil engineering work, installation of the iron and the length of the shut-down of the neutrino facility.

(*) The name BRIC-F is used throughout for convenience. It arises as this is the sixth version of a shield which started as a quick "bricolage" to correct the shielding at 400 GeV.

The purely geometric considerations of required stopping power and available material are shown in table 3 as a function of angle to the target λ and azimuthal ϕ. The "minimum shielding" is the amount of material in g/cm^2 required to give a background of $\sim 1\mu/m^2/10^{13}$ p on the BEBC-EMI; the data is taken from the curves of ref. [3] averaged over the appropriate mixture of iron and earth. The "present shield" is as calculated from the program description. It can be seen that the bulk of the additional iron has to be added above the centre line of the beam and at the sides with a maximum of 112 m to fill the "hole" at 3 mr.

(a) Layout

The additional shielding is added in two places, between pit 5 and the end of the present iron, and after the building 274 (fig. 8).

After building 274 there is sufficient place to add the 36 m of iron required on the beam axis. The lateral size of this block has to be sufficient to intercept the 3 mr ray from the target, ± 2.5 m at this point. An additional metre of shield is added below the beam axis to compensate for material not added underneath the shield between pits 5 and 7. The installation of this 5 x 6 x 36 m block is complicated by the existence of the side foundations of the West Area. A schematic drawing of the installation is shown in fig. 9, with the cross section at AA', the start of the block, shown in fig. 10.

From pit 5 until the end of the present shield ($\sim$ 73 m) the present disks of diameter 2.5 m are replaced by, or extended to, a block 5 m x 3.6 m. A criterion of the ease of civil engineering was that the floor of the present tunnel and the rails of the installation system should not be touched. This request has been more or less complied with and is the reason for the extra depth of the block behind building 274. However, between pits 6 and 7 an additional 50 cm of iron should be added below the present shield. The cross sections of this shield are shown in fig. 11.

The total weight of this new shielding is 7600 t for the part behind building 274 and 6600 t between pit 5 and the end of the present shield. To this 14 200 t of new iron should be added the 2600 t of the disks installed at present.

(b) Performance

The configuration of iron described above approximates quite well to the requirements given in table 3. There is adequate material to stop all linear muon trajectories up to angles of $\sim$ 5 mr (it is probably reasonable to collimate the hadrons of a 450 GeV wide-band beam at this angle). To study the overall performance of the shield including multiple scattering etc., the technique of calculation described above has been applied. The background rates predicted are shown in table 4. These rates are quite acceptable, about a factor of two less than those currently measured at 350 GeV. As seen previously, for antineutrinos the background of μ^+ is the worst, about five times more than the μ^- background in the ν beam. This merely reflects the π^+/π^- production spectra and is a common feature of all passive shields.

The distribution of the intensity of μ^+ background in the 450 GeV $\bar{\nu}$ beam is shown at the EMI plane in fig. 12. The azimuthal distribution can be clearly seen, the BEBC visible volume is well in the shadow of the iron shield, but there are "hot spots" of intensity above and to the right, looking upstream. The source of this remaining leakage can be seen in fig. 13 which shows the transmission of μ^+ through the shield as a function of λ at the target, integrating over all azimuthal angles. There is a clear maximum at 2-3 mr from the target, i.e. 3-4 mr in space (the magnetic deflection of the horn and reflector is typically $\sim$ 1 mr) due to these trajectories missing the main absorber after building 274. An extra metre of iron above and to the side would reduce the background further.

From this study of an optimized passive shield it can be concluded that at the expense of nearly 15 000 t of new iron and considerable civil engineering it is possible to build a valid neutrino shield for

450 GeV and $\sim 10^{13}$ protons per pulse. At 450 GeV the muon background would be such as to allow operation of BEBC and the BEBC-EMI, but it could not be expected to increase the primary energy much above this value.

4.2 TOROID - A partially magnetic shield

The main defect of the shield described above is purely practical, the very large radius, and corresponding cost of the iron shield required to intercept the muons diverging from the target. The principle of the toroid shield is to maintain the advantages of a passive shield, but to minimise the amount of iron required by using a toroidal magnet, acting as a lens, to focus the diverging trajectories back into the main shielding block after building 274. This philosophy is quite unlike that of a purely magnetic shield [4] which tries to bend all trajectories away from the detector without stopping them. A purely magnetic extension of the shield was briefly tried, but abandoned because it was impossible to ensure that no trajectory could reach the detector even after passing through the system of two or three magnets. In addition the problems of multiple Coulomb scattering, and in particular nuclear scattering, make it difficult to guarantee that such a system would work.

The operation of the toroid shield is much simpler in concept, a schematic drawing is shown in fig. 14. The magnet is 6 m in diameter, with a central hole of 2 m diameter; a maximum field of 12 kG over the 10 m length will give the required 12 Tm bending power. Particles with angles up to 5 mr which miss the present shield will be deflected back to the axis and into the absorber, or away from the detector. Particles already in the shield will pass through the 2 m diameter field-free hole and remain in the shield up to the absorber. With the magnetic horns in operation this effect is enhanced as the position of the magnet and the internal radius of the hole is optimised such that most of the particles in the magnet are of one charge, while those in the hole are of the other. Also, because of the structure of

the present shield, those particles of the wrong sign which do enter the magnet are of lower momentum and are deflected strongly away from the detectors at BEBC or WA1.

The main absorber block of 36 m of iron is again required, as in the previous shield design. However, the focusing effect of the magnet allows a much smaller cross section of 4 x 4.5 m^2 to be used, saving considerably on the cost.

(a) Layout

The optimum position to place the toroidal magnet is just after pit 5, fig. 15. This allows the focused ray at 3 mr to pass through the 112 m of iron required to stop it, table 3. Also, pit 5 is sufficiently far from the target to have a good spatial separation of the positive and negative muons due to the deflection of the horn and reflector.

The magnet proposed is of a very simple construction, there is no need to have good field uniformity. It would consist of disks of iron 6 m in diameter, 2 m internal diameter, perhaps 10 cm thick. A hundred of these disks mounted together make the unit of 10 m long. The magnet is energised by four coils mounted as shown in fig. 14, each coil is made from an aluminium bar 10 x 10 cm in cross section and the four coils are connected in series to a single power supply, $\sim$ 50 kW. The current density in the coil is kept low $\sim$ 1 amp/mm^2 to avoid the need for any external cooling. The voltage is also low to avoid any problems with insulation. In general the design of the magnet is as simple and robust as possible to avoid any problems of maintenance. To maximise the stopping power on axis the central hole of the magnet is plugged with iron disks, leaving an air gap to avoid distorting the field inside the toroid.

The civil engineering associated with the installation of this 1800 t magnet on the beam axis at pit 5 are clearly not trivial, however it is much less than the installation of the extra iron from pit 5 to the end of the present shield, proposed in the previous solution.

The main absorber block 4 x 4.5 x 36 m is placed after building 274 as before. The problems of installation are similar to those discussed previously, however, again the block is much smaller $\sim$ 4700 t compared with the 7600 t of absorber for the "BRIC-F" shield.

(b) Optimization

Unlike the passive shielding where the parameters of the design are fixed by purely geometrical considerations, the toroidal magnet solution has a few options, for example the radius of the internal hole of the toroid, which have to be optimized. Clearly the criteria for optimization is to minimise the background at a reasonable cost. However it has also been chosen to equalise the background rate for the ν and $\bar{\nu}$ beams to avoid the present situation of being forced to run these beams at different energies. As mentioned previously this option is not possible with a purely passive shield due to the unequal π^+, π^- production rates.

The means available to compare the performance of the shield and adjust the parameters has been to compute the rate and distribution of backgrounds on the BEBC-EMI using the program already described. The average trajectories of muons of both charges leaving the target is shown in fig. 16. The position of the magnet is fixed by the need to have at least 112 m of iron to intercept the deflected 3 mr ray. The bending power of the toroid should be such as to deflect the 3 mr ray on to the axis at the absorber, an angle of 15 mr. The maximum momentum of a muon at this point on the toroid is $\sim$ 230 GeV/c giving a bending power of 11.5 Tm. The result of the complete calculation is shown in fig. 17, the variation of the total background intensity with the field and polarity of the toroidal magnet for the 450 GeV $\bar{\nu}$ beam. It can be seen from the figure that turning on the field should give a very substantial reduction in background, about a factor of hundred, up to 12 Tm after which the gain levels off. This is clearly understandable, as once the muons are focused on the absorber further power in the magnet will not reduce the background. Because of its small size the

visible volume of BEBC sees the same background for either polarity of the magnet, however for the wrong polarity the EMI has very much more background.

To understand the effect of the diameter of the hole in the toroid, reference must be made to fig. 18 which shows the variation of intensity of background as a function of angle at the target λ, for the proposed shielding layout. For negative muons from the 450 GeV $\bar{\nu}$ beam, i.e. rays which are focused by the horns and defocused by the magnet, fig. 16(b), there is a strong maximum of transmission at $\sim$ 2.4 mr. These muons which have multiple scattered outwards, intercept the magnet, are defocused past the absorber and reach the detector. If the radius of the hole is increased to avoid this problem, positive muons at about 1.0 mr have a chance to pass the magnet undeflected and multiple scatter out of the main absorber block to the detectors. The variation of this radius is shown in fig. 19 against the total transmission of these competing positive and negative rays in the overlap region at the inside edge of the magnet. An optimum value of the radius at 100 cm can be seen from this plot.

The two maxima in fig. 18 for positive muons at small angles < 0.6 mr and at about 2 mr correspond to cases where particles have multiple Coulomb scattered away from the beam axis, or at 2 mr, towards the beam axis, missed the magnet, and followed trajectories round the absorber to the detector. The intensity of this background has been minimised by adjusting the size of the final absorber block, and positioning its centre slightly, 50 cm, above the beam axis.

(c) Peformance

The total predicted background rates for the ν, $\bar{\nu}$ and no horn beam at 450 GeV/c primary proton momentum are shown in table 5. They are completely satisfactory, about half those of the purely passive shield, in the worst case of an antineutrino beam. The distribution of background for those muons focused by the magnet is rather central, like that seen at present in the 400 GeV data (fig. 6) but of much lower intensity.

The background of the other charge, focused by the lens and defocused by the magnet, is of much higher total intensity, especially in the ν beam, but is located far from the beam axis, typically 7-10 m and little backscatters into the EMI.

Various checks of the stability of the toroid shield design parameters have been made by computing the backgrounds for different conditions of the beam. Neither moving the target horizontally by up to $\pm$ 60 cm, nor changing the focusing power of the horn and reflector have shown any deviation in the quality of the shield.

This design study of a partially magnetic, partially passive neutrino shield has shown that a good neutrino shield can be built with considerable economies in the amount of iron and civil engineering effort required.

5. CONCLUSION

This study of the West Area neutrino beam shielding has shown that the leakage of muons observed at 350 and 400 GeV/c primary proton momentum can be easily understood as due to a lack of stopping power of the shield at certain critical angles, $\sim$ 3 mr from the target. The techniques used in the computation of this background have been applied to the design of an extension of the shield to 450 GeV/c proton momentum. Two optimized shielding designs have been studied in detail. The first, a conventional passive iron shield is possible but expensive in iron and civil engineering effort. The second, a partially magnetic, partially passive iron design gives a better performance in terms of background levels, and considerable economies in the cost of construction. It is outside the scope of this note to discuss the technicalities of installation and details of costing of the two designs. However it is evident that the designs have evolved within the constraints of these technical problems. The net effect of this has been to produce a first design of a practical magnetic shielding which could in principle be extended to higher primary proton energies.

ACKNOWLEDGEMENTS

The scope of the work reported in this note developed from the meetings of a group (to study the problems of the West Area neutrino shield) under the chairmanship of P. Lazeyras. The author gratefully acknowledges the useful discussions with members of this group, especially with H.W. Atherton on the computation of energy loss of muons at high energy and with B. Bianchi on the possibilities, and many cost estimates, of the installation work involved.

REFERENCES

[1] J. Ranft, Leipzig University Report KMU-HEP 75-03 (1975).

[2] C. Richard-Serre, Yellow Report CERN 71-18 (1971).

[3] H.W. Atherton, private communication.

[4] R. Hartmann and H. Leutz, Nucl. Instr. Meth. 126 (1975) p.165.

TABLE 1

Momentum GeV/c	Mean range $gm/cm^2 \times 10$		Material for weight of 10^{-4}
	Total E loss	Ions. E loss	$gm/cm^2 \times 10^{-4}$
200	7.6	8.1	9.5
400	12.8	16.0	16.7
500	15.0	21.0	19.5

TABLE 2

Ev	Measured rates/10^{12} on EMI	in BEBC	Predicted/10^{12} ppp on EMI	in BEBC
350 ν	36	1.0	23.	1.3
$\frac{\mu^+}{all}$	-	3%	0.7%	.5%
350 $\bar{\nu}$	103	$\sim$ 8.0	129.	8.0
330 $\bar{\nu}$	44	0.8	13.5	0.65
$\frac{\mu^+}{all}$		$\sim$ 100%	$\sim$ 100%	$\sim$ 100%
350 No horn	$\sim$ 77	$\sim$ 4	31	1.7
$\frac{\mu^+}{all}$			85%	84%
400 ν	456.	30	1292	95
			1.8%	1.2%

TABLE 3

λ mR	Minimum shield required gm/cm^2 x 10^5	Present shield gm/cm^2 x 105			Additional iron required metres		
		Range of ϕ			Range of ϕ		
		-90^o - $+90^o$	150^o - 210^o	90 - 150^o 210 - 270^o	-90^o + 90^o	150^o - 210^o	90 - 150^o 210 - 270^o
0 - 1.0	1.75	1.57	1.64	1.61	36	2	28
1.5	1.75	1.63	1.72	1.65	24	6	20
2.0	1.75	1.51	1.87	1.83	0	0	0
2.5	1.75	1.43	1.72	1.72	64	6	6
3.0	1.72	1.16	1.58	1.36	112	34	72
3.5	1.68	1.27	1.48	1.44	82	40	48
4.0	1.65	1.30	1.48	1.47	70	34	36
4.5	1.63	1.31	1.50	1.50	64	26	26
5.0	1.58	1.32	1.51	1.51	52	14	14
6.0	1.48	1.33	1.52	1.52	30	0	0

TABLE 4

BRIC-F Shield

Predicted background/10^{12} protons

450 GeV	μ +		μ -	
	In BEBC	On EMI	In BEBC	On EMI
ν	10^{-4}	10^{-2}	.4	12.
$\bar{\nu}$	1.6	55.5	10^{-3}	10^{-2}

TABLE 5

TOROID Shield

Predicted background/10^{12} protons

450 GeV	μ +		μ -	
	In BEBC	On EMI	In BEBC	On EMI
ν	.3	29	.3	4.5
$\bar{\nu}$	1.7	23	$7\ 10^{-2}$	5.9
no horn + field	6.210^{-2}	3.3	$2.8\ 10^{-2}$	8.2

FIGURE CAPTIONS

Fig. 1 Distribution of momentum left from a 400 GeV/c muon after ionisation energy loss of the present neutrino shield in: (a) vertical scan in angle from the target, (b) horizontal scan. The shaded portion shows the effect of the modification to the shield made in May 1977.

Fig. 2 Predicted and measured momentum of $\mu^{\pm}$ from the 400 GeV ν beam. The dashed curve shows the underestimate of the momentum made by using the mean total energy loss.

Fig. 3 Schematic drawing of the effects of ignoring the distortion of the multiple scattering envelope due to the shadowing effect of different densities of absorber.

Fig. 4 Predicted intensity distribution of background μ^{-} from the 350 GeV ν wide-band beam at the BEBC-EMI plane. The size of the EMI chambers projected onto this plane are shown.

Fig. 5 Comparison of the predicted background intensities with those measured at the EMI. The measured rates on the EMI chambers have been corrected for cosmic and ν induced background and projected onto a plane normal to the neutrino beam.

Fig. 6 Predicted intensity distribution for μ background in 400 GeV ν beam. Intensity contours at 10, 50 and 90 are shown as dashed curves. The scale per 20 x 20 cm cell is arbitrary.

Fig. 7 Comparison of predicted and measured intensity at 400 GeV ν wide-band beam corrected as in fig. 5.

Fig. 8 Plan view of the neutrino shield installation showing the position of the additional passive iron shield.

FIGURE CAPTIONS (Cont'd)

Fig. 9 Detail of the layout of the main absorber block for the BRIC-F shield at the side of the West Area.

Fig. 10 Cross section of the BRIC-F shield at the start of the main absorber block, showing the position of the foundations of the West Area.

Fig. 11 Cross section of the additional iron for the BRIC-F shield between pits 5-6 and between pits 6-7.

Fig. 12 Predicted intensity distribution at the EMI plane for μ^+ from the 450 GeV $\bar{\nu}$ beam, BRIC-F shield.

Fig. 13 Intensity of background for the BRIC-F shield as a function of polar angle from the target λ.

Fig. 14 Schematic drawing of the toroidal magnet and position of the final 4 x 4.5 x 36 m absorber.

Fig. 15 Plan view of the neutrino shield installation showing the position of the toroidal magnet and the main absorber block.

Fig. 16 Indicates the mean trajectory of muons through the toroid shield for: (a) parent pions defocused by the lens system giving muons focused by the magnet, and (b) pions focused by the lens and muons defocused by the magnet.

Fig. 17 Variation of background intensity with bending power of the toroidal magnet.

Fig. 18 Variation of the background intensity of μ^+ and μ^- from the 450 GeV/c $\bar{\nu}$ beam, toroid shield, as a function of the polar angle from the target.

FIGURE CAPTIONS (Cont'd)

Fig. 19 Variation of the background intensity at the EMI for critical angles, 1. mr for μ^-, 2.4 mr for μ^+ in the 450 $\bar{\nu}$ wide-band beam, toroid shield, as a function of the radius of the internal hole in the toroidal magnet.

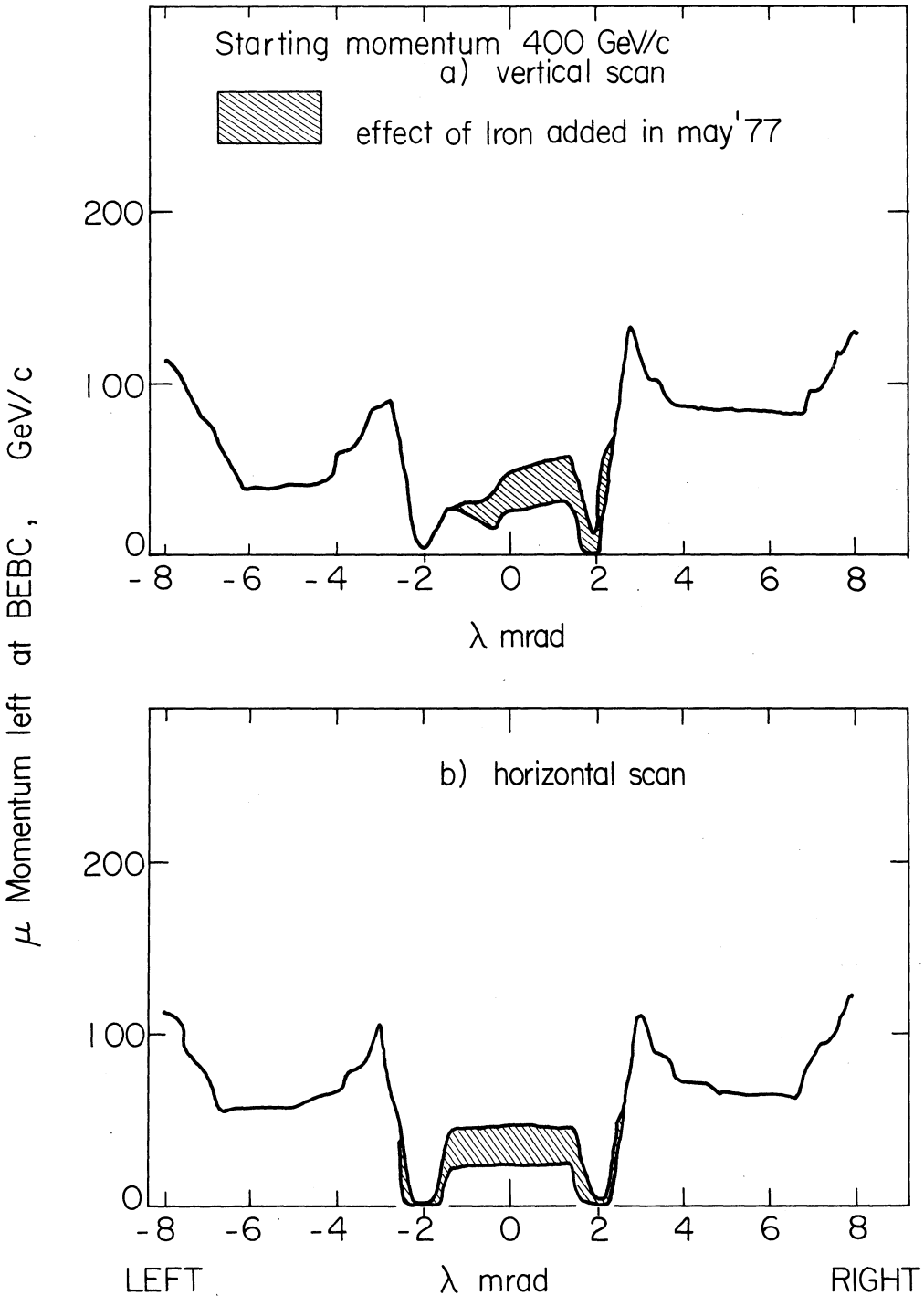
Starting momentum 400 GeV/c
a) vertical scan
effect of Iron added in may '77
200
100
0
-8
-6
-4
-2
0
2
4
6
8
λ mrad
μ Momentum left at BEBC, GeV/c
b) horizontal scan
200
100
0
-8
-6
-4
-2
0
2
4
6
8
LEFT
λ mrad
RIGHT

fig. 1

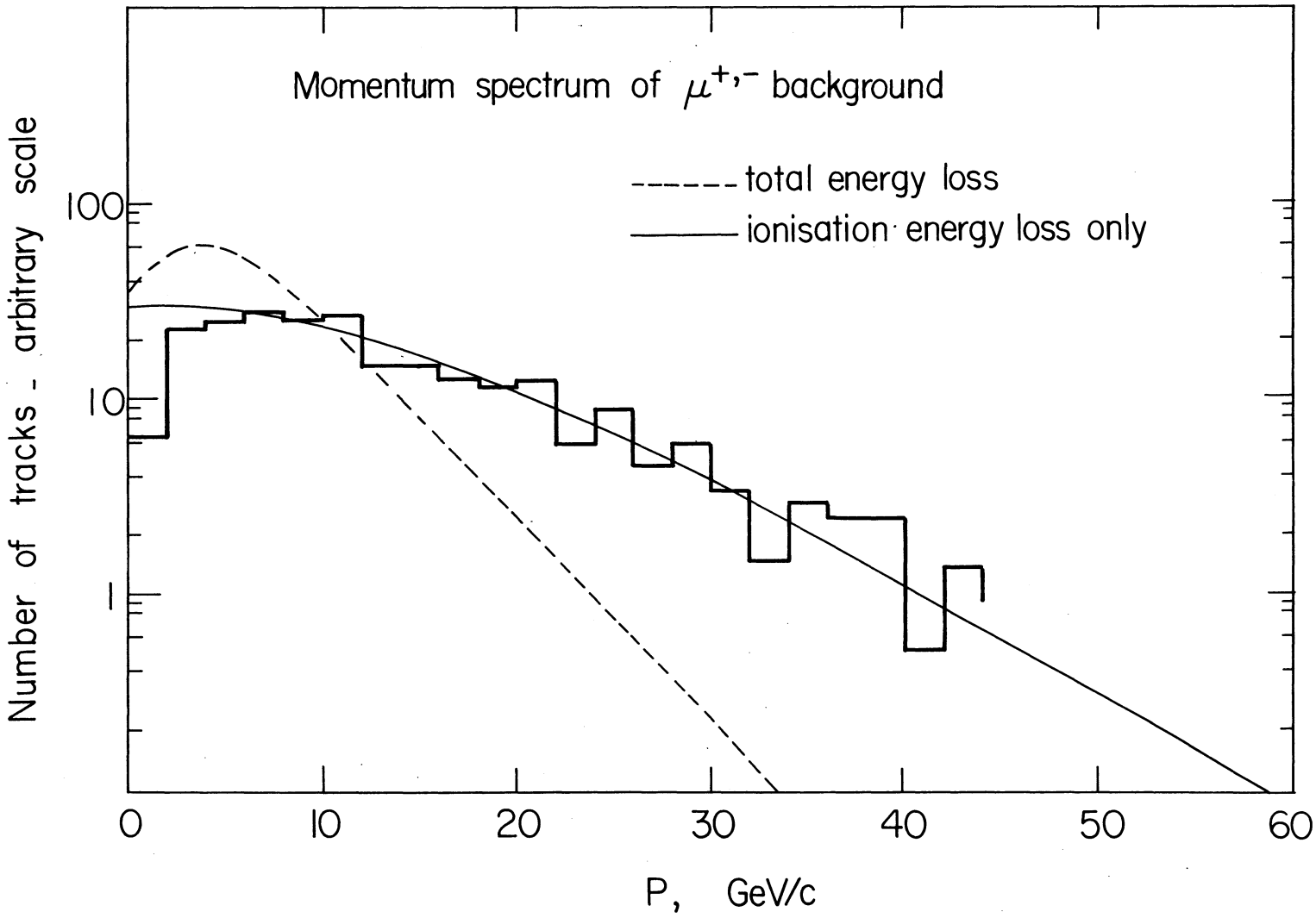
Momentum spectrum of $\mu^{+,-}$ background
total energy loss
ionisation energy loss only
Number of tracks - arbitrary scale
100
10
1
0
10
20
30
40
50
60
P, GeV/c

fig. 2

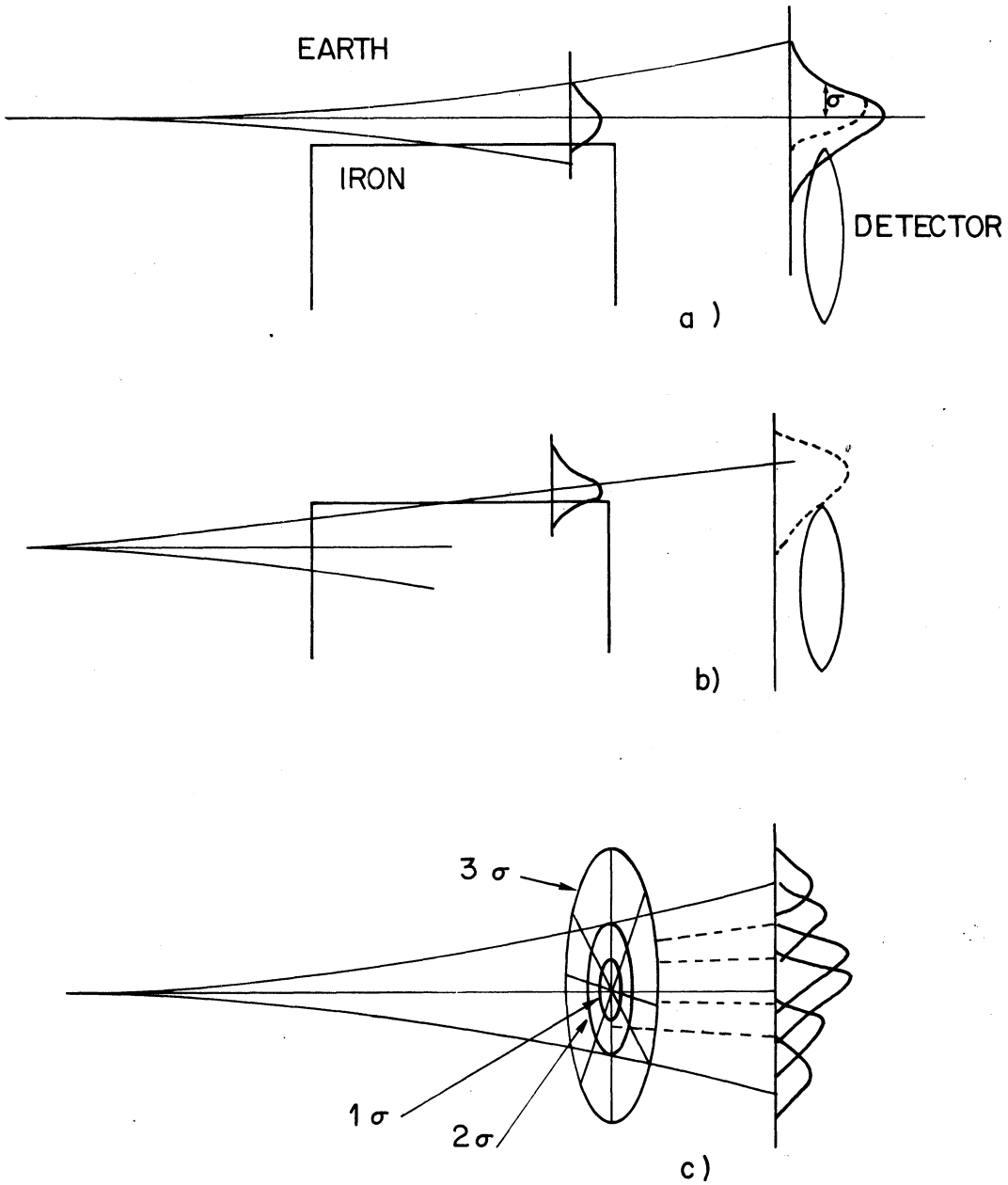

fig. 3

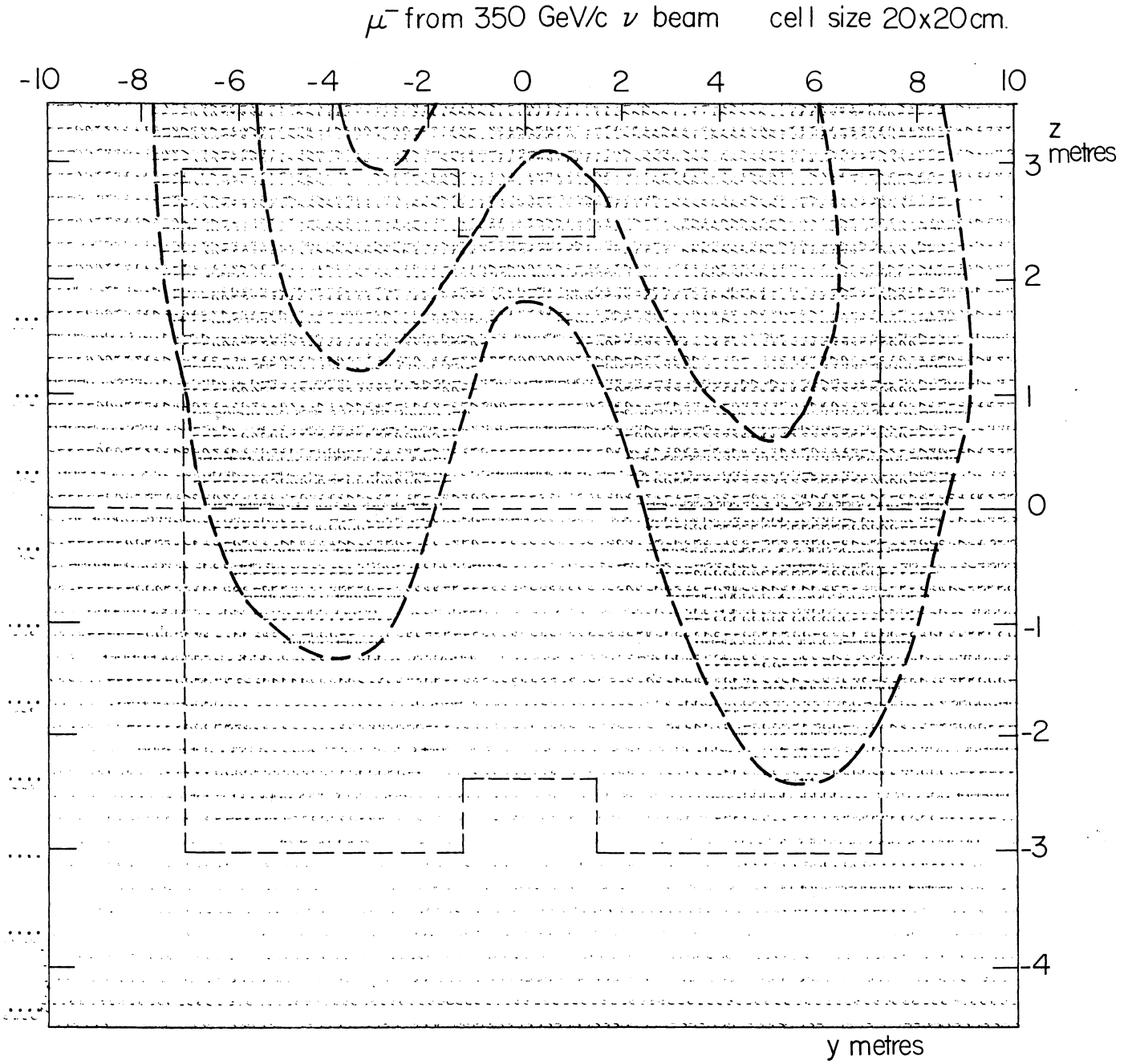
μ^- from 350 GeV/c ν beam cell size 20x20cm.
-10
-8
-6
-4
-2
0
2
4
6
8
10
z metres
3
2
1
0
-1
-2
-3
-4
y metres

fig. 4

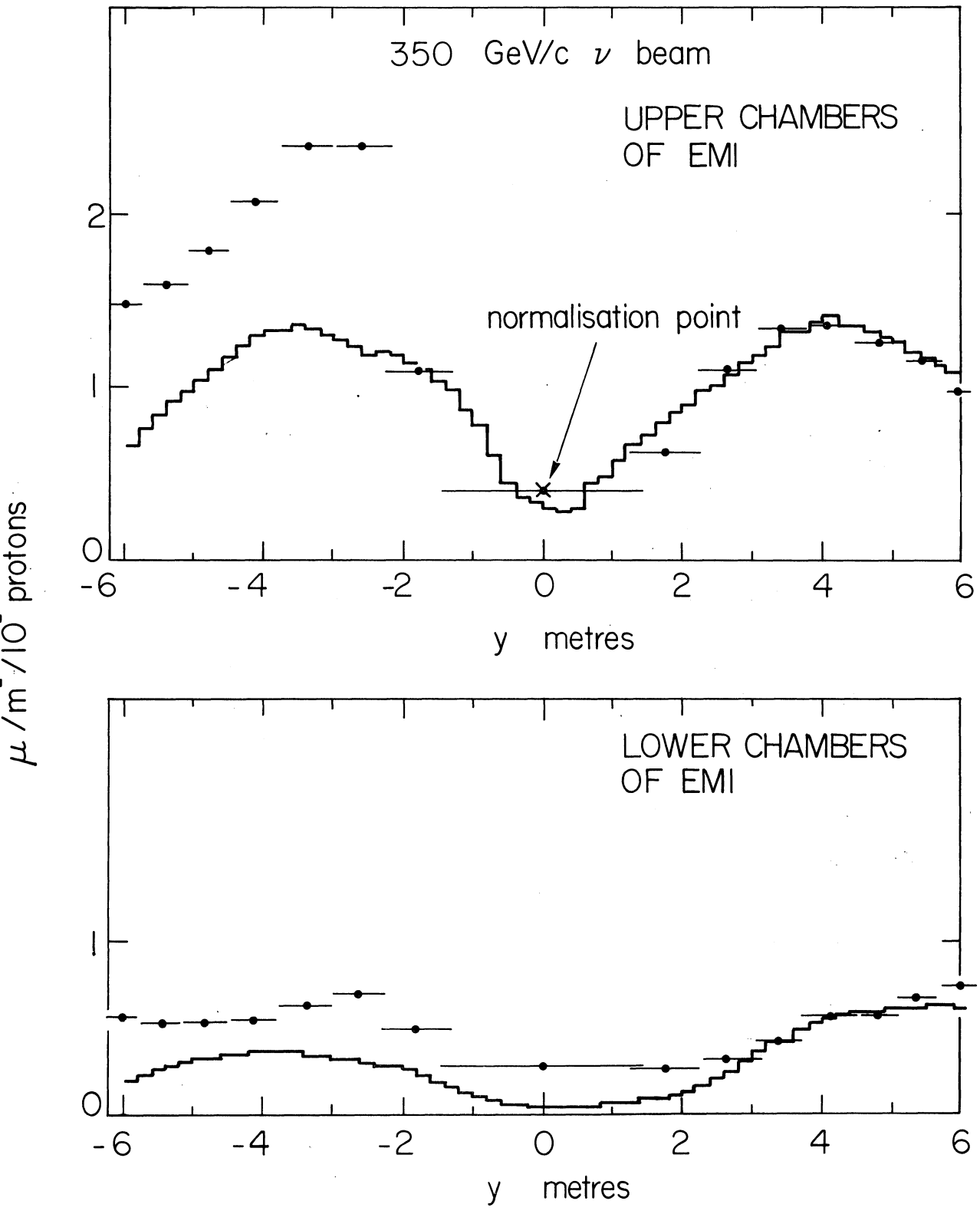
350 GeV/c ν beam
UPPER CHAMBERS
OF EMI
normalisation point
2
1
0
-6
-4
-2
0
2
4
6
y metres
μ/m²/10² protons
LOWER CHAMBERS
OF EMI
1
0
-6
-4
-2
0
2
4
6
y metres

fig. 5

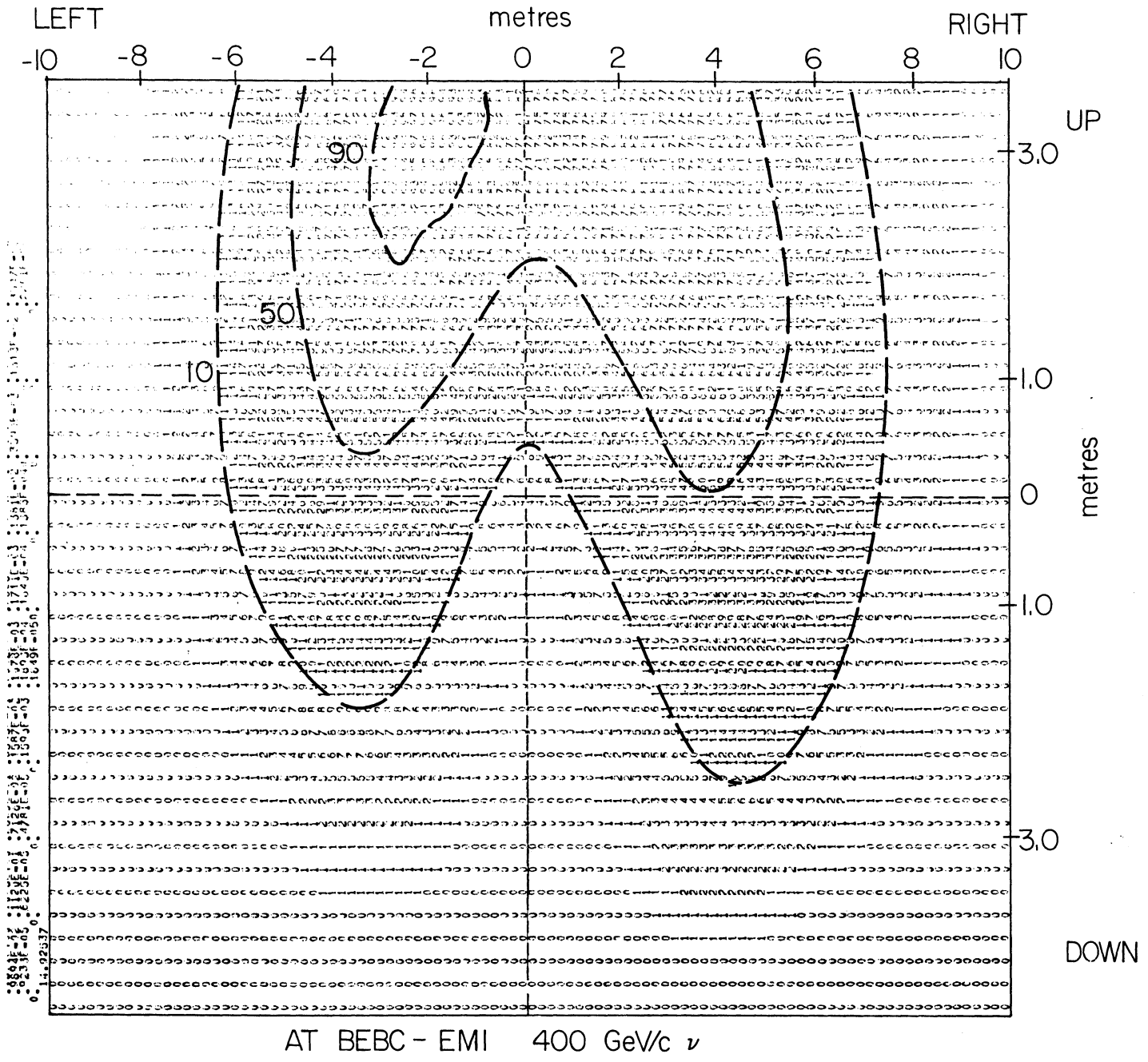
LEFT
metres
RIGHT
-10
-8
-6
-4
-2
0
2
4
6
8
10
UP
3.0
1.0
0
metres
1.0
3.0
DOWN
90
50
10
AT BEBC - EMI 400 GeV/c ν

fig. 6

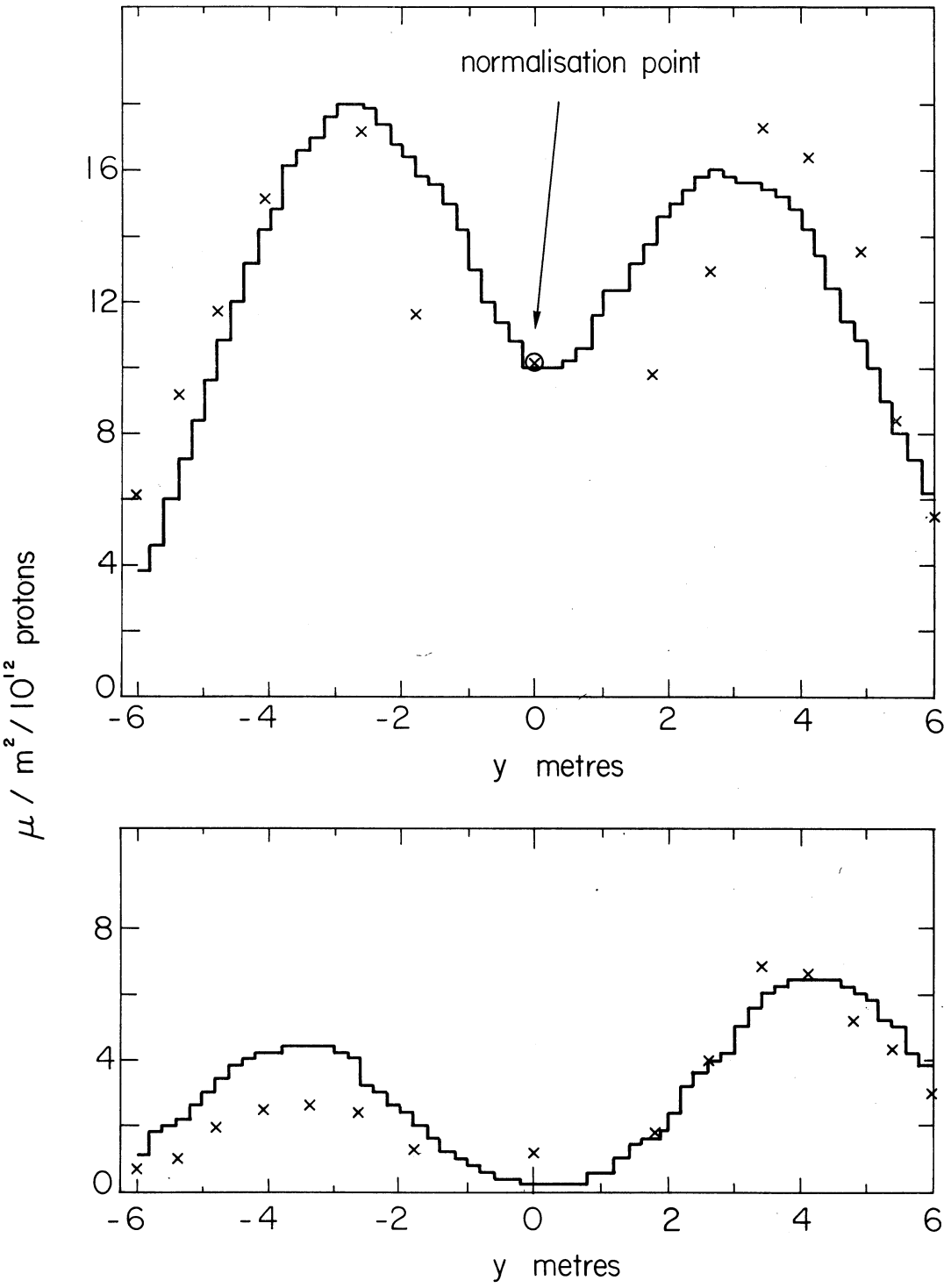
normalisation point
16
12
8
4
0
-6
-4
-2
0
2
4
6
y metres
μ / m² / 10¹² protons
8
4
0
-6
-4
-2
0
2
4
6
y metres

fig. 7

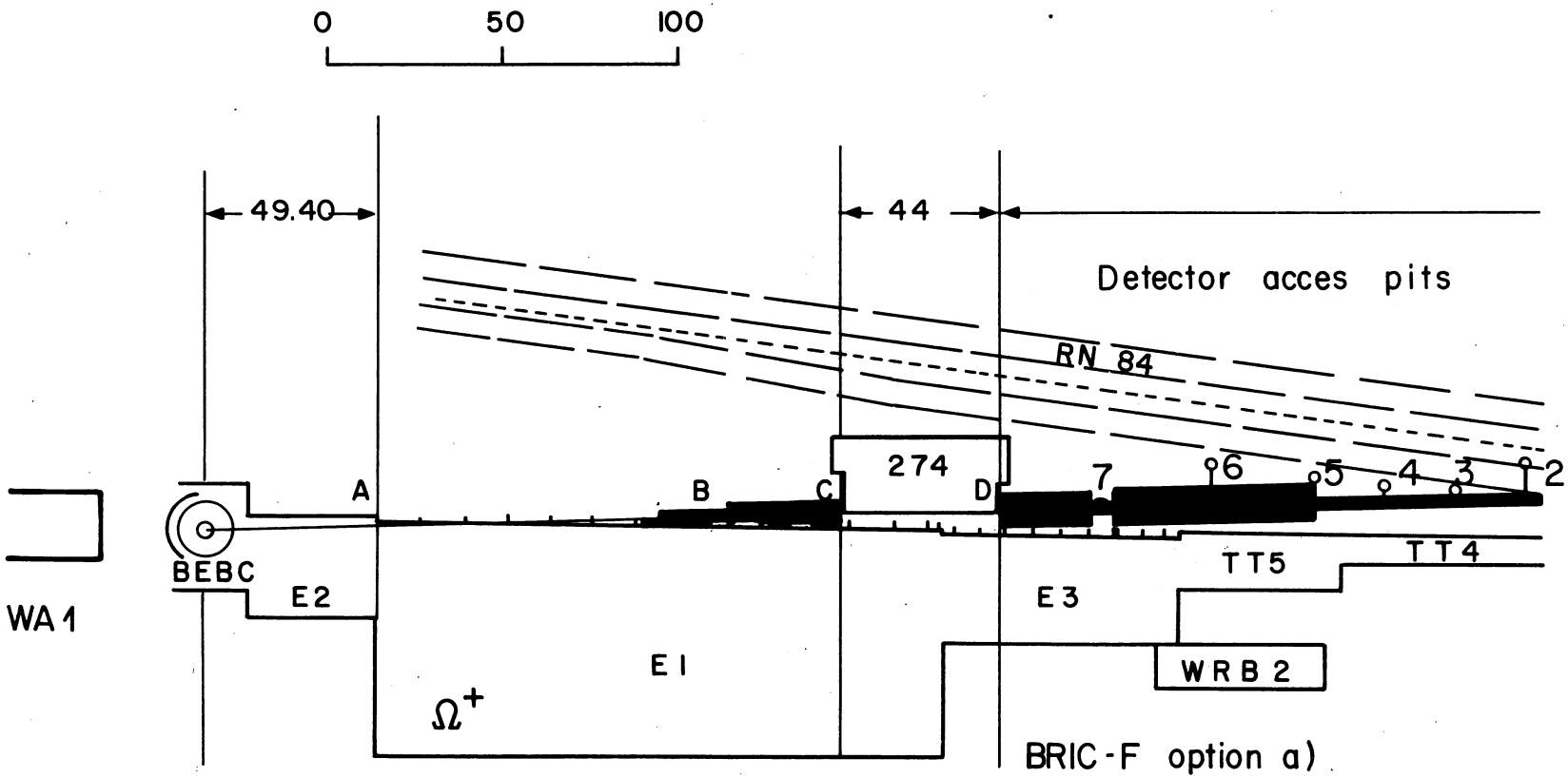
0
50
100
49.40
44
Detector acces pits
RN 84
274
A
B
C
D
7
6
5
4
3
2
BEBC
WA 1
E2
E1
E3
TT5
TT4
WRB 2
Ω+
BRIC-F option a)

fig. 8

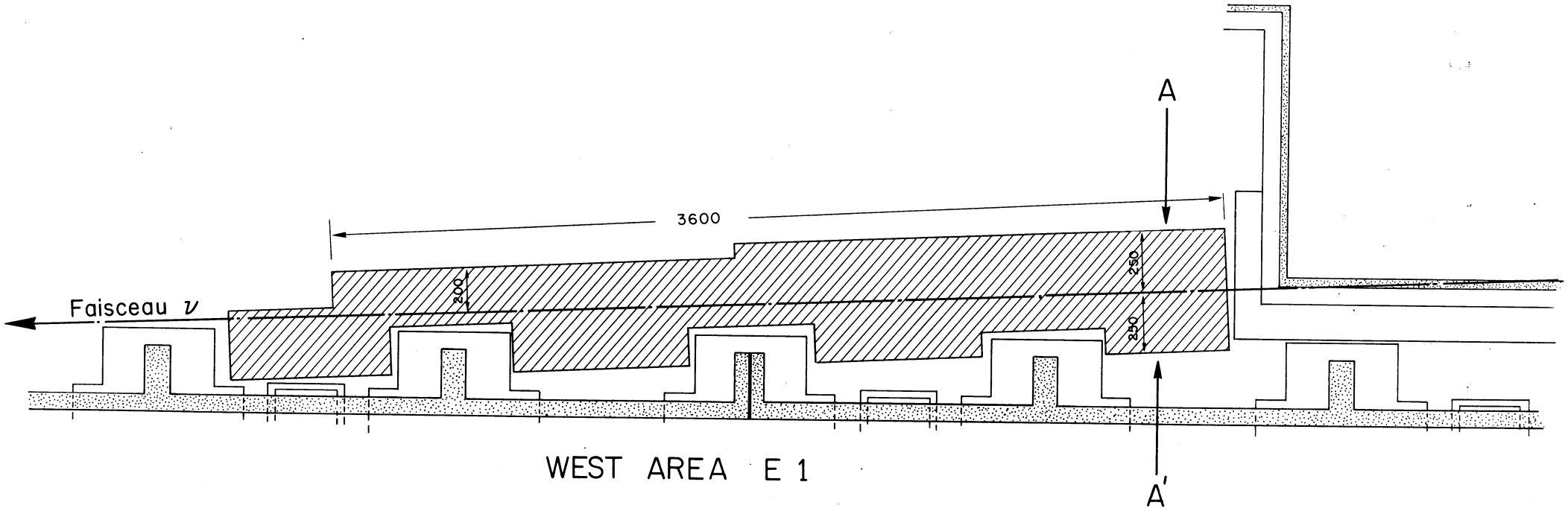

Fig. 9

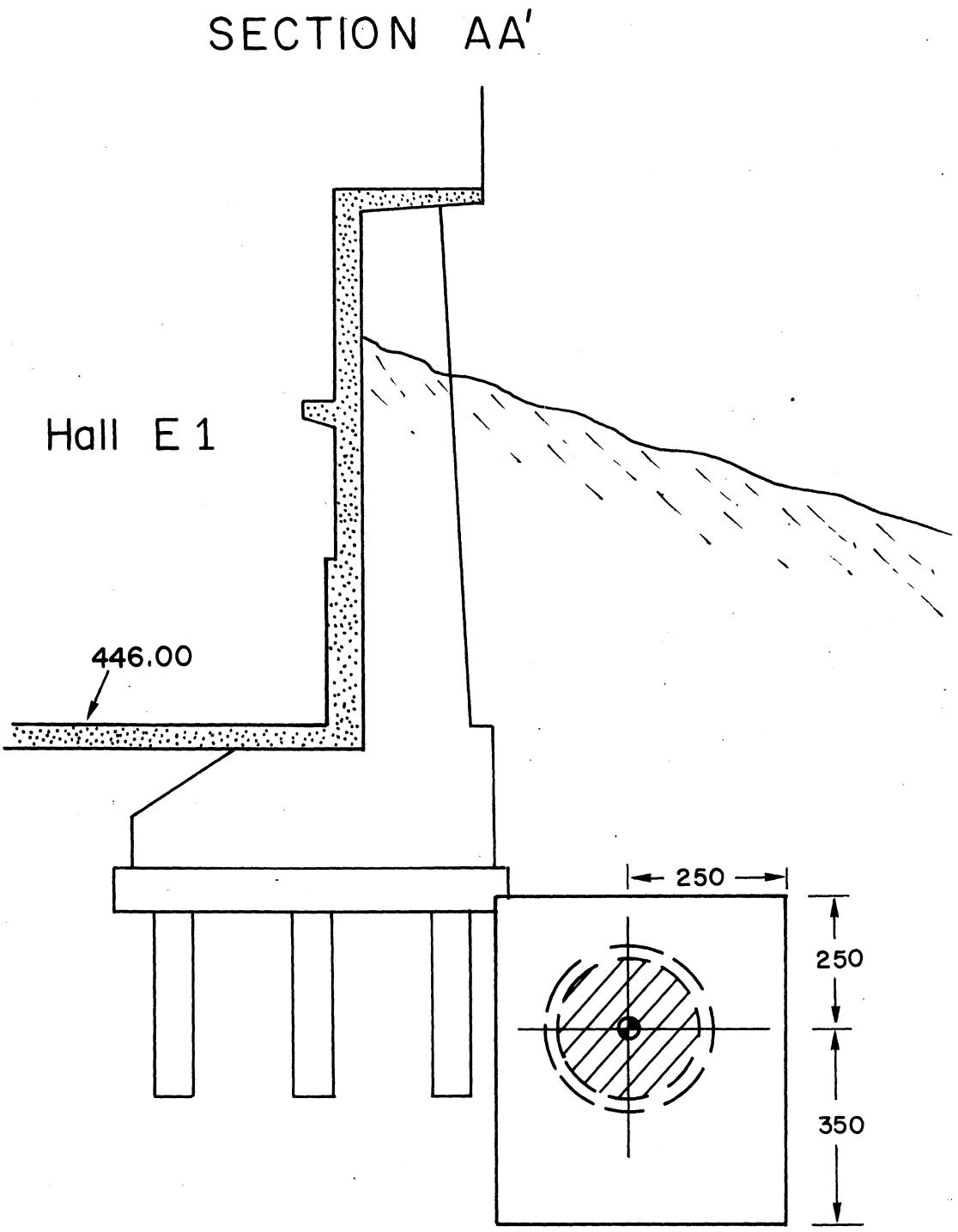

Fig. 10

PASSIVE IRON SHIELD

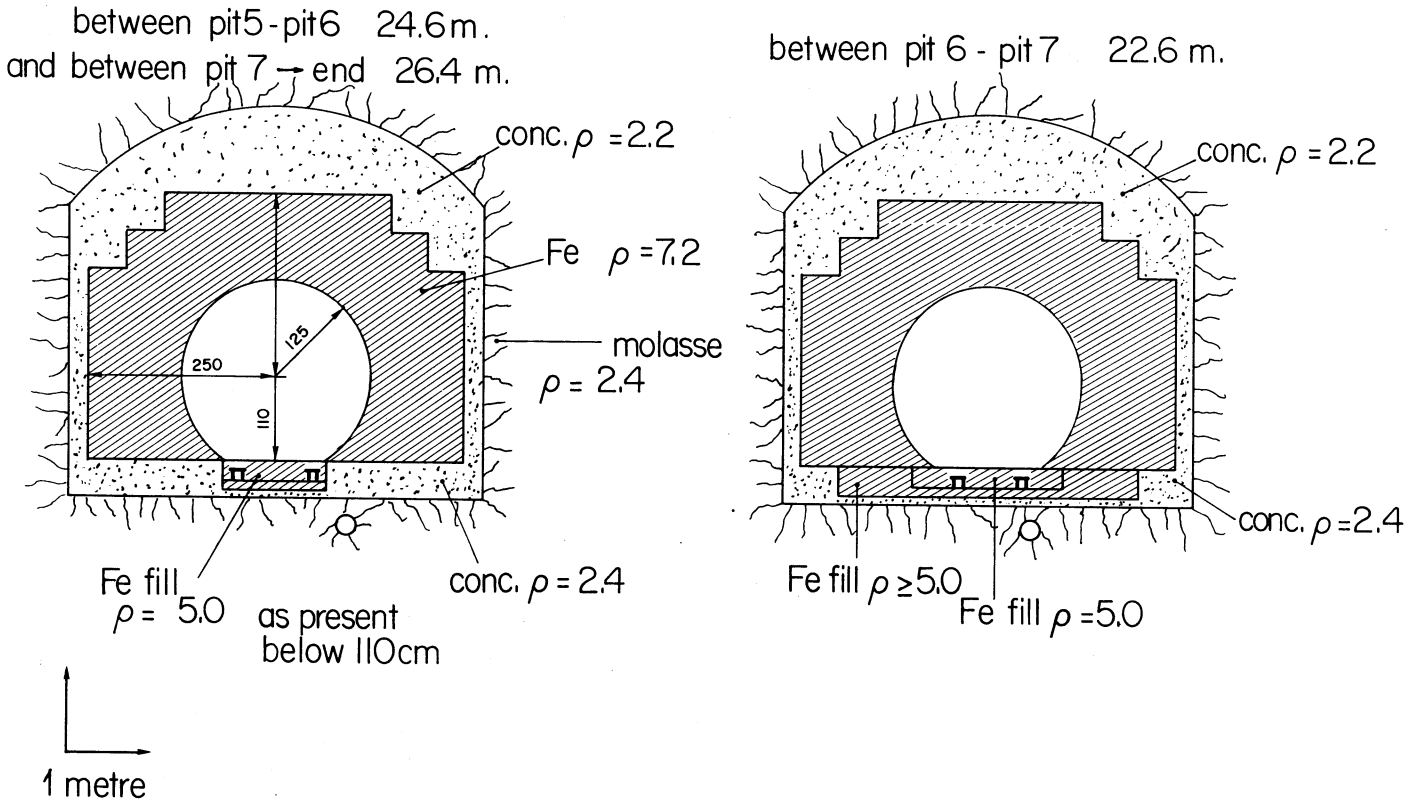

fig.11

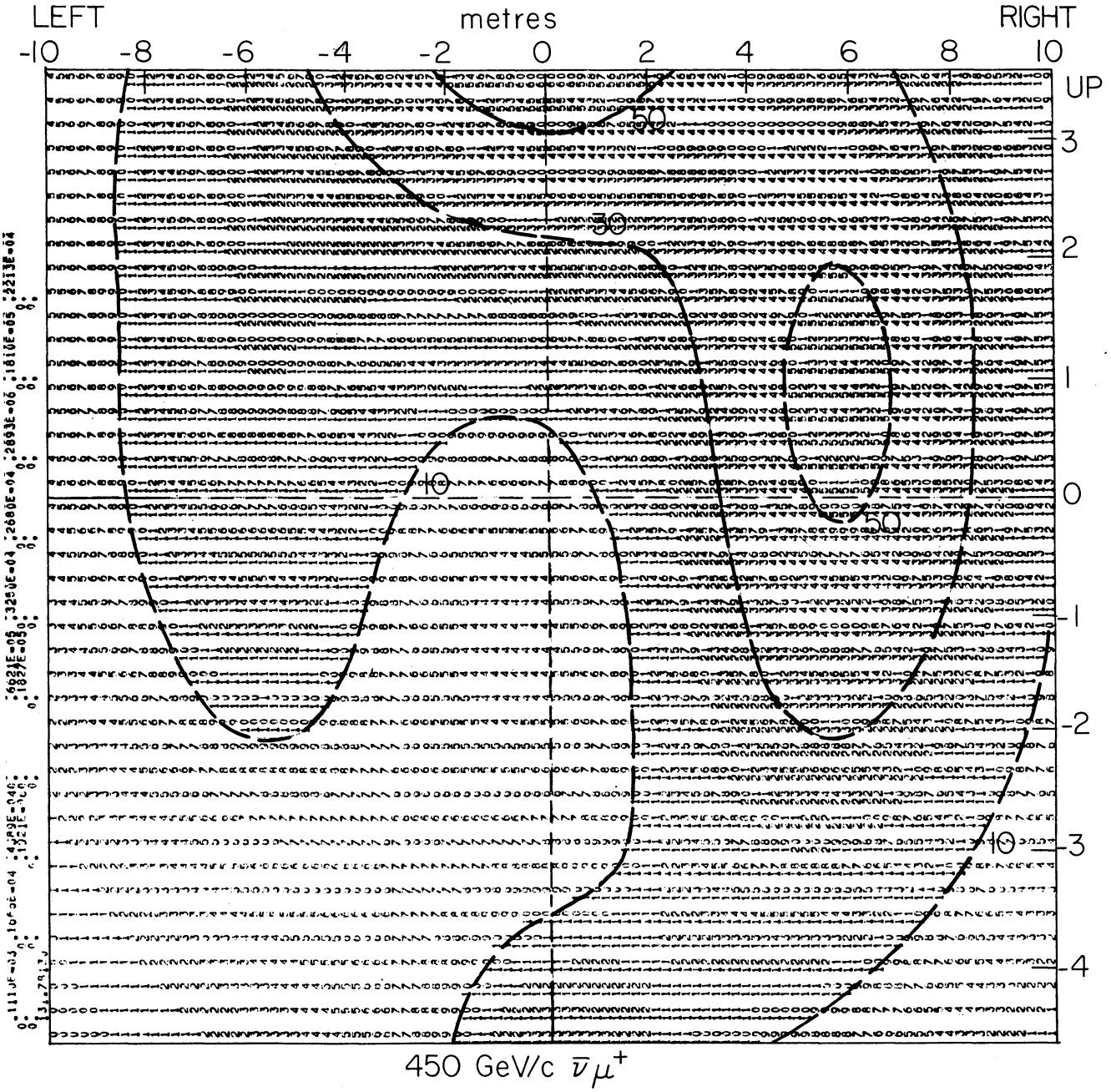
LEFT
metres
RIGHT
-10
-8
-6
-4
-2
0
2
4
6
8
10
UP
3
2
1
0
-1
-2
-3
-4
50
30
10
10
50
10
450 GeV/c $\bar{\nu}\mu^+$

fig.12

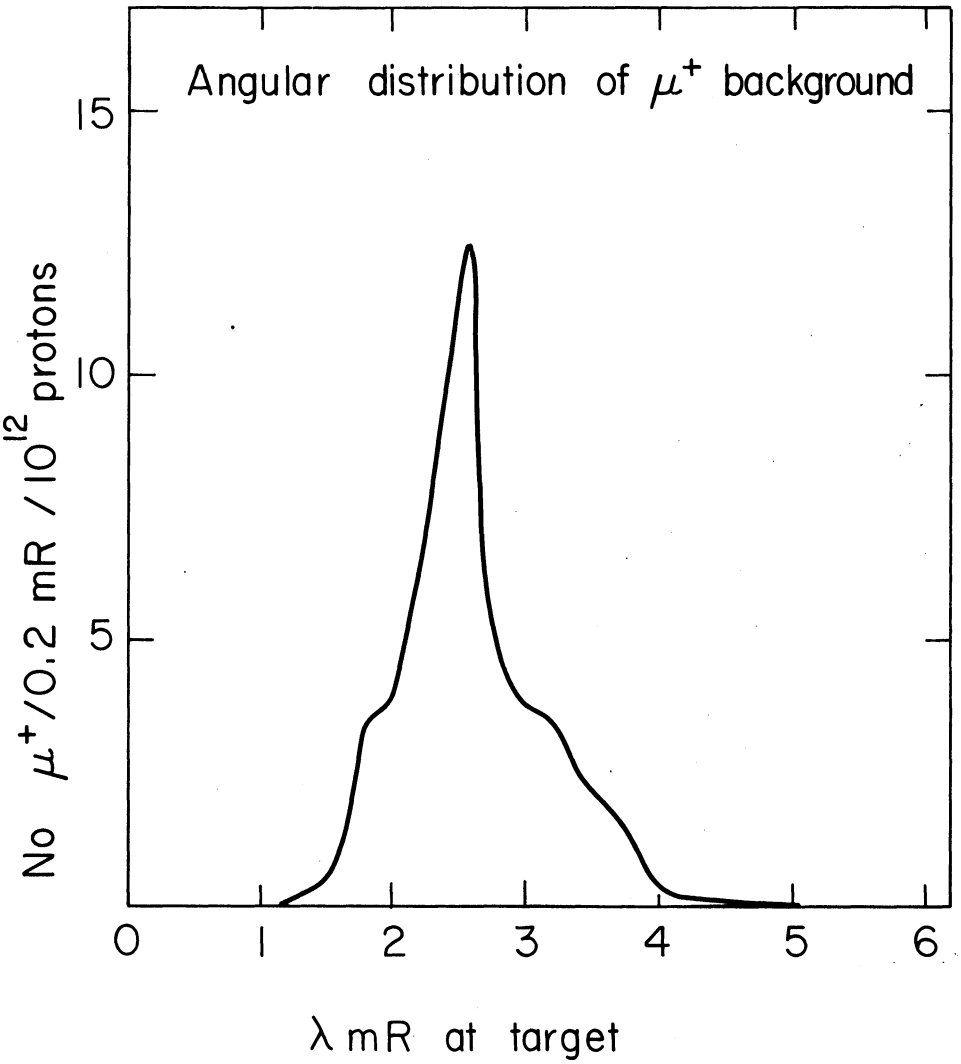
Angular distribution of μ^+ background
No μ^+/0.2 mR / 10^{12} protons
15
10
5
0
1
2
3
4
5
6
λ mR at target

fig.13

Layout of toroid magnet and absorber

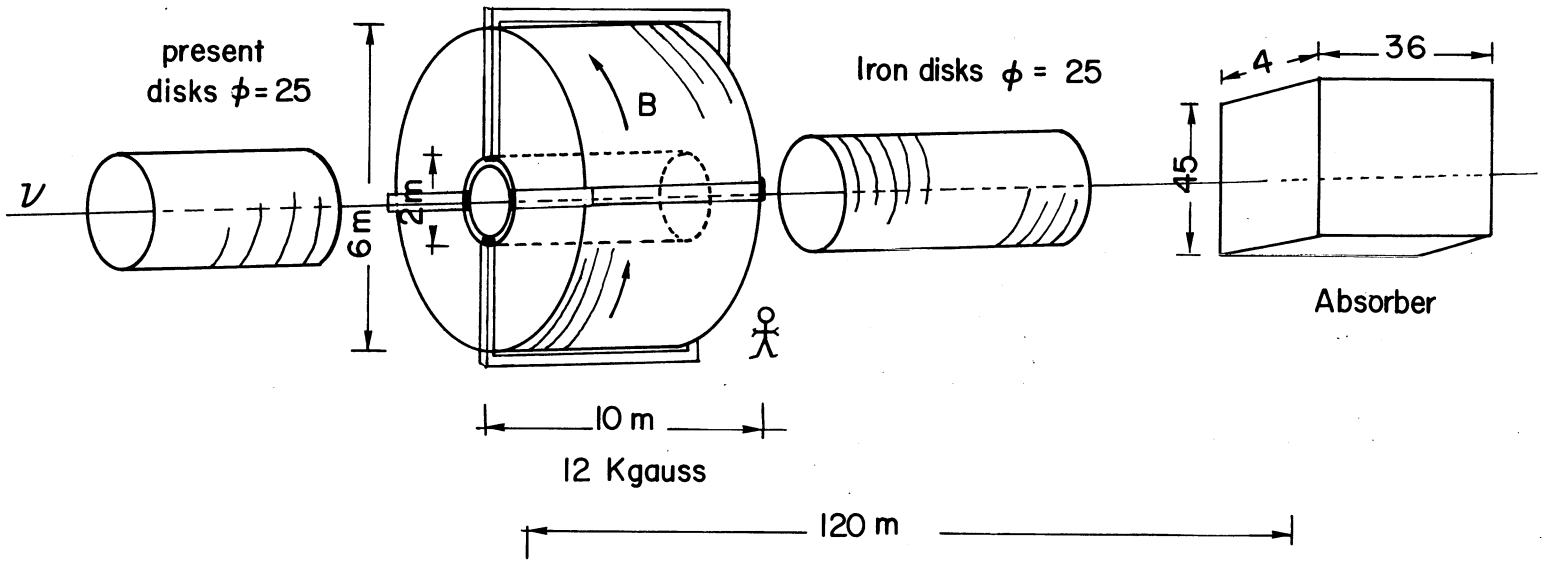

fig.14

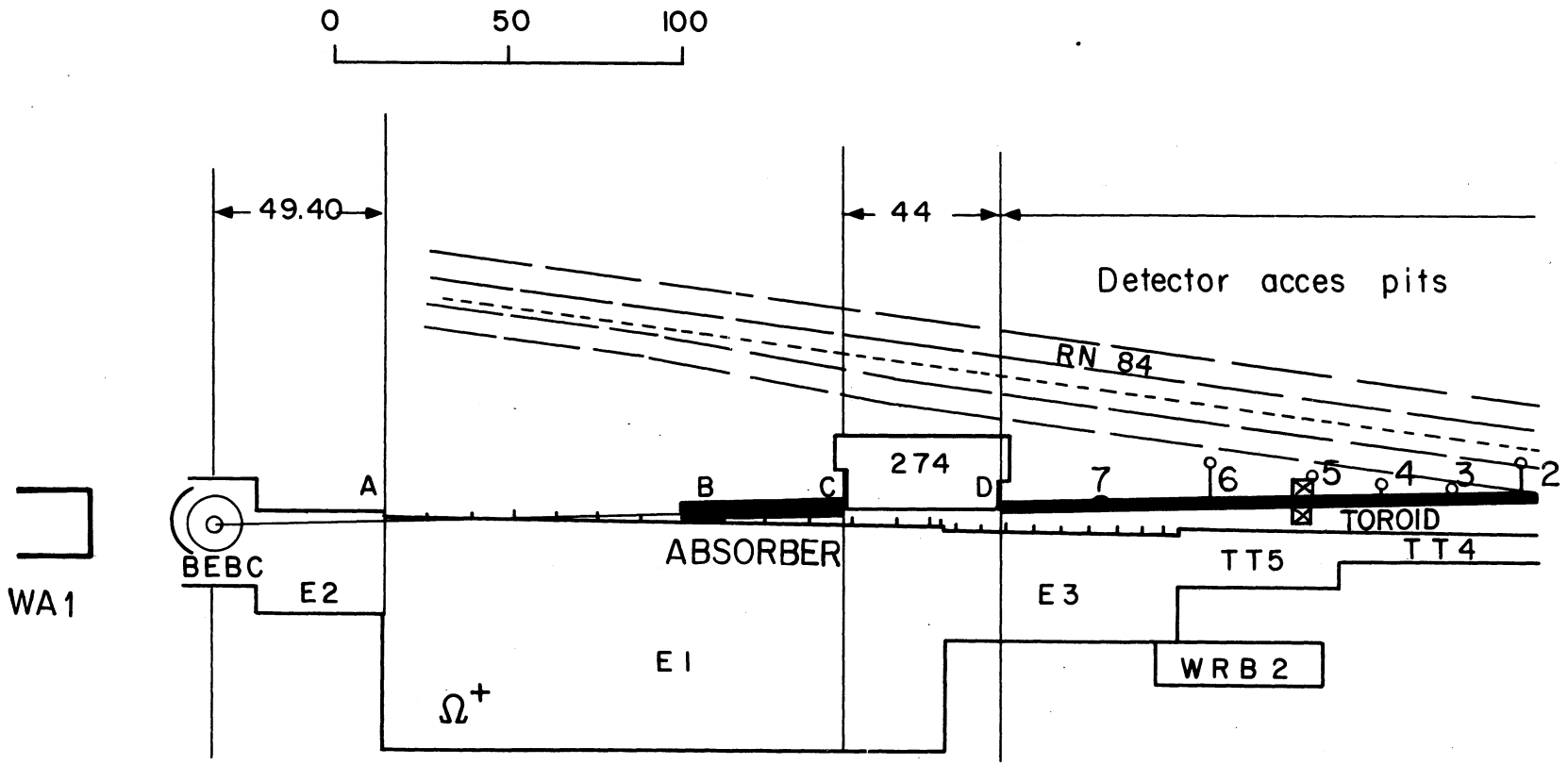

TOROID option b)

fig.15

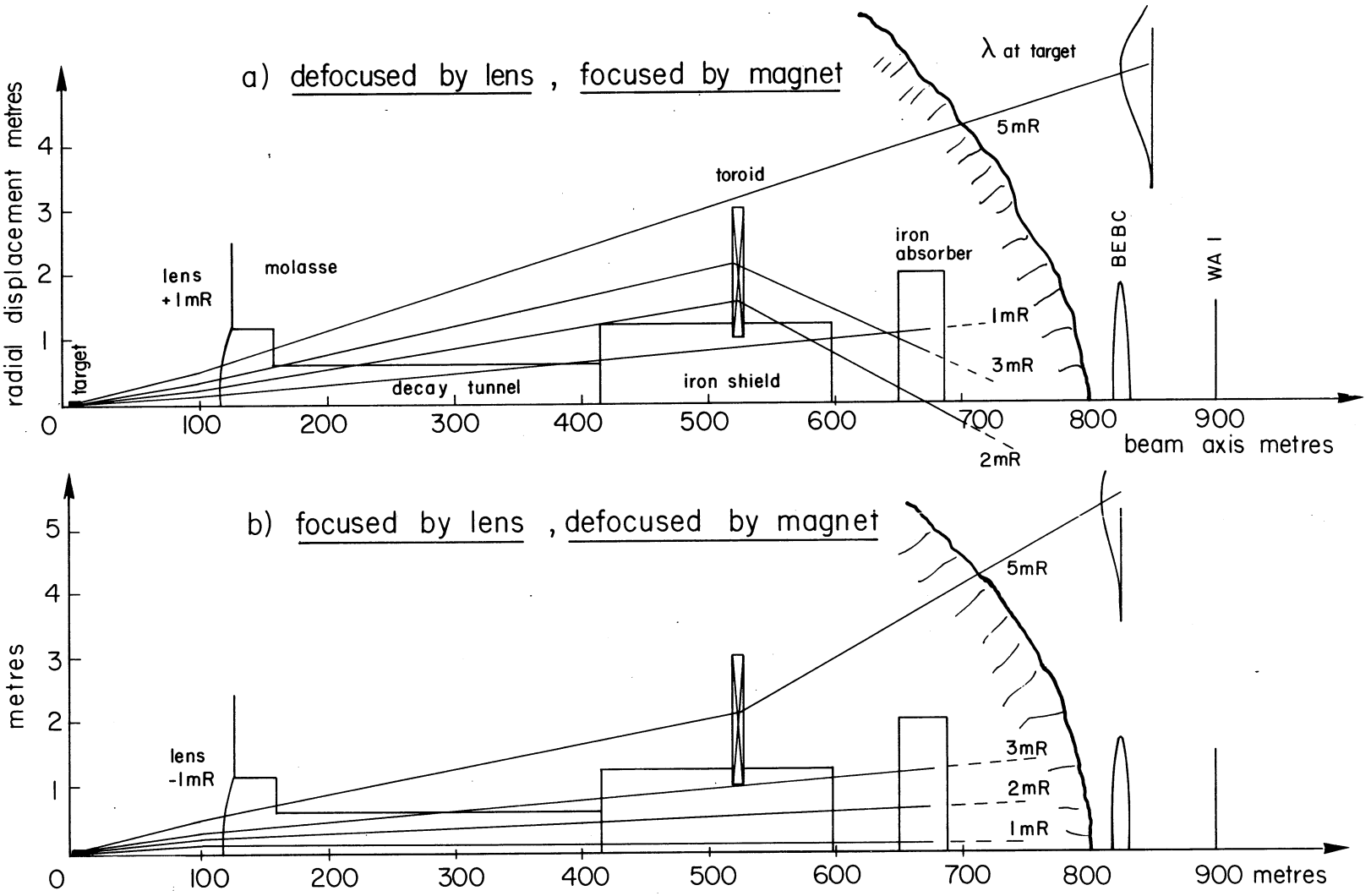
a) defocused by lens , focused by magnet
radial displacement metres
λ at target
5mR
toroid
iron absorber
BEBC
WA I
lens +1mR
molasse
target
1mR
3mR
decay tunnel
iron shield
2mR
0
100
200
300
400
500
600
700
800
900
beam axis metres
b) focused by lens , defocused by magnet
metres
5mR
lens -1mR
3mR
2mR
1mR
0
100
200
300
400
500
600
700
800
900 metres

fig.16

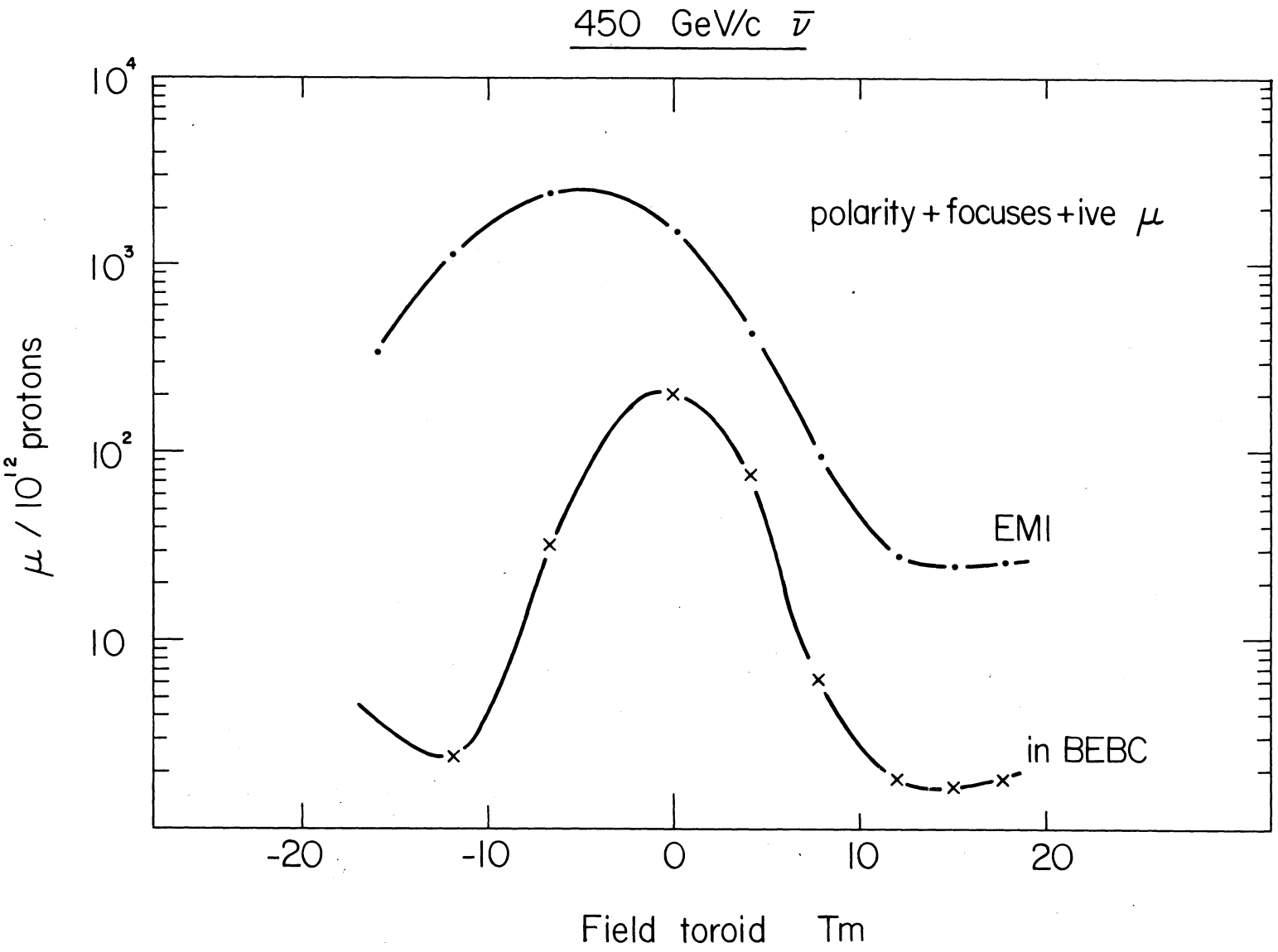
450 GeV/c $\bar{\nu}$
10^4
10^3
10^2
10
μ / 10^{12} protons
polarity + focuses + ive μ
EMI
in BEBC
-20
-10
0
10
20
Field toroid Tm

fig.17

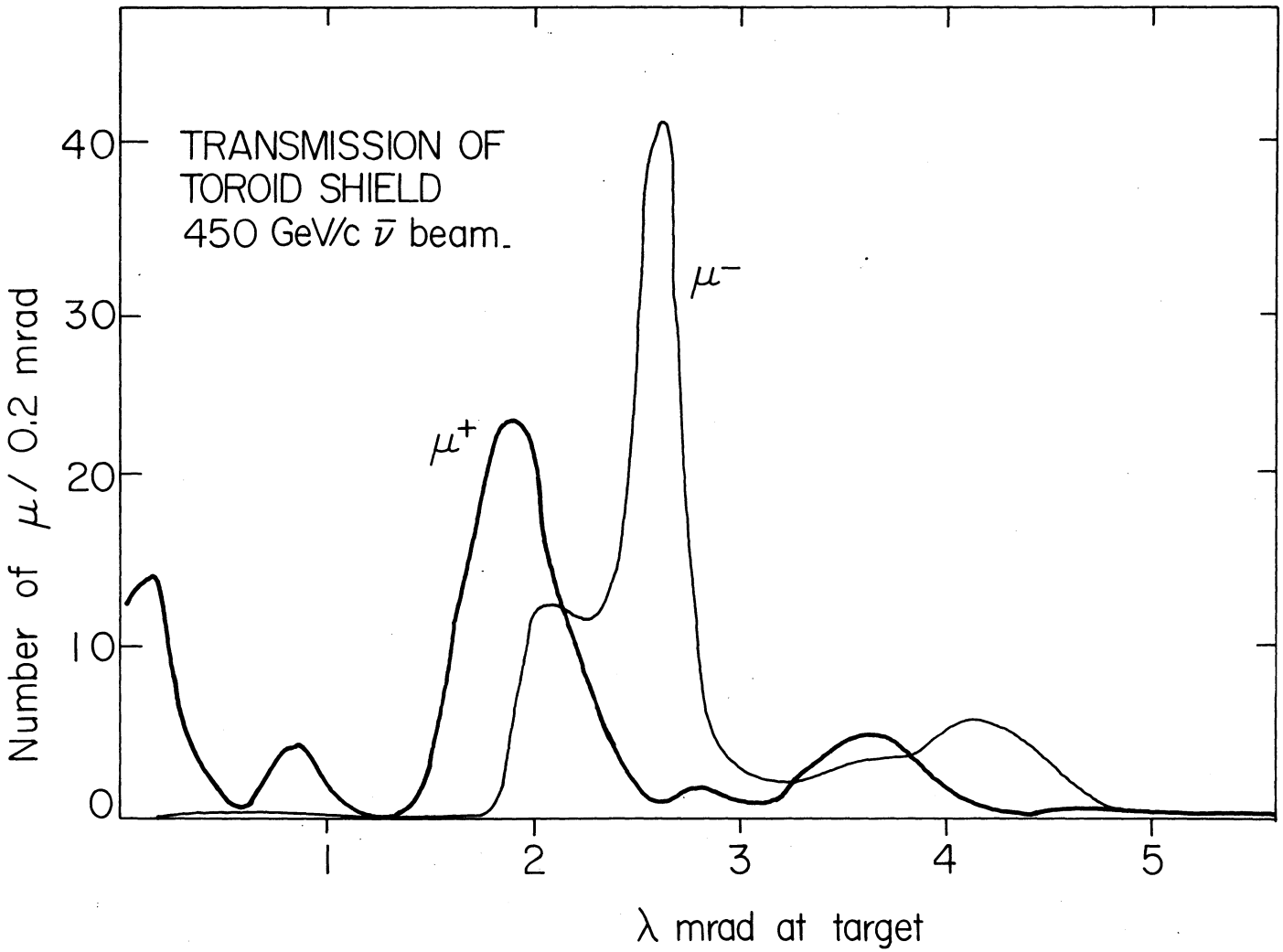
TRANSMISSION OF
TOROID SHIELD
450 GeV/c $\bar{\nu}$ beam.
μ^-
μ^+
Number of μ / 0.2 mrad
0
10
20
30
40
1
2
3
4
5
λ mrad at target

fig.18

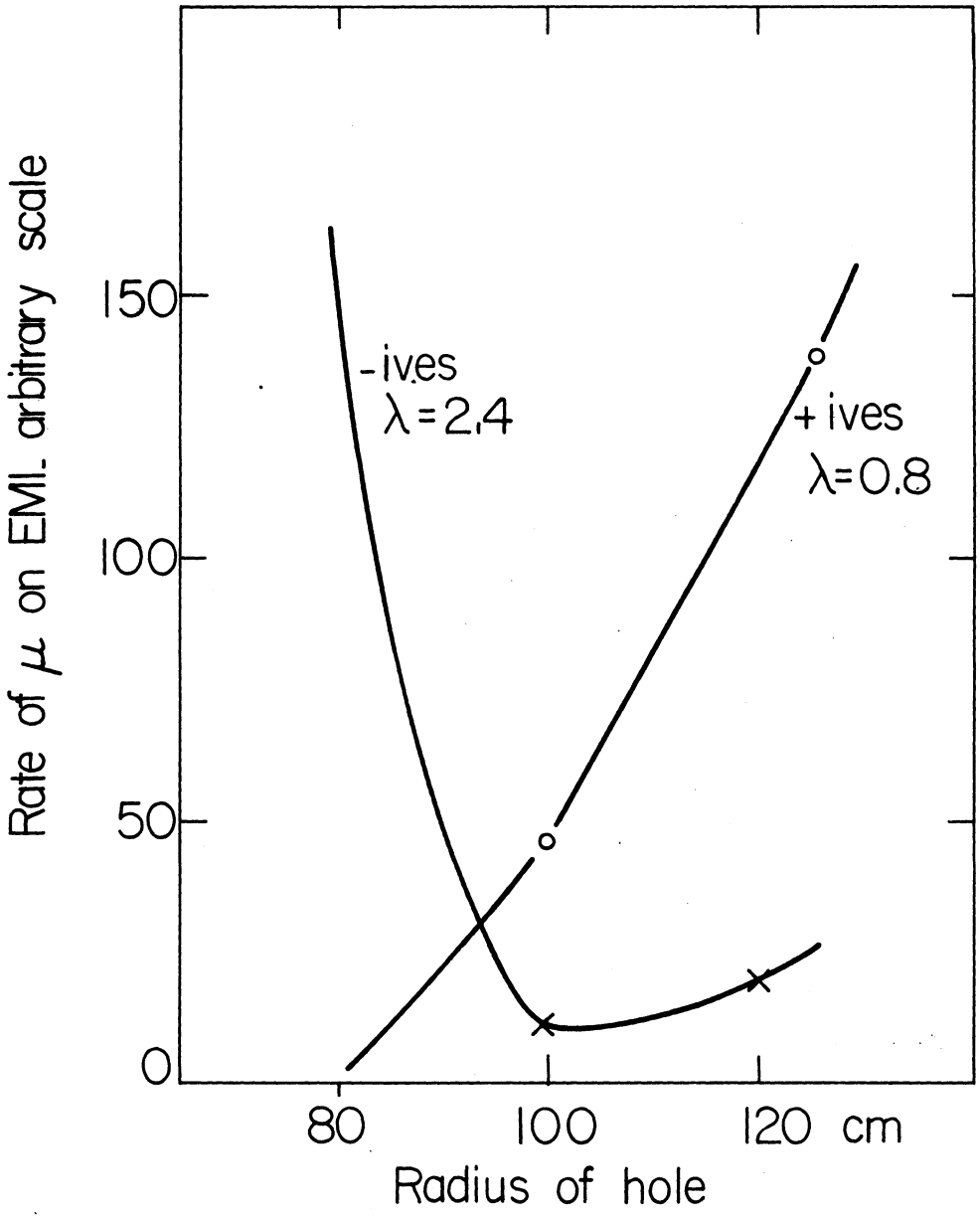
Rate of μ on EMI. arbitrary scale
150
100
50
0
-ives
λ=2.4
+ives
λ=0.8
80
100
120 cm
Radius of hole

fig.19